ELSEVIER

Comput. Methods Appl. Mech. Engrg. 137 (1996) 285–306

Computer methods in applied mechanics and engineering

# Adaptive meshing for dynamic strain localization

Arghya Deb[a], Jean H. Prevost[a,*], Benjamin Loret[b]

[a]*Department of Civil Engineering and Operations Research, Princeton University, Princeton, NJ 08544, USA*
[b]*Institut de Mecanique de Grenoble, Domaine Universitaire, B.P. 53X, 38041 Grenoble Cedex, France*

Received 28 August 1995

**Abstract**

A mesh enrichment procedure is developed to capture the shear band for strain localization in elasto-(visco)-plastic solids. The enriched mesh comprises four and five noded quadrilateral elements which can be adaptively refined in the localized zone. The criterion for mesh adaption combines three well-known localization characteristics to predict the onset of localization in individual elements. A modified procedure for transferring state variables between two successive refined meshes is proposed. The procedure is tested by solving several sample problems. Consistent and stable solutions are obtained. In particular, shear band widths and plastic strains are found to converge to stable values. The results are compared with solutions using the enriched displacement procedure defined in [1]. The efficiency of the global adaptive scheme is tested on initial- and boundary-value problems that involve different material properties and geometries.

## 1. Introduction

The numerical simulation of strain localization has to face two important difficulties. The first difficulty is related to the loss of hyperbolicity of the dynamical equations of motion and the resulting ill-posedness of the problem. This is usually alleviated by having recourse to various regularization procedures [2–7]. Though involving radically different mechanisms, each of the aforementioned works aims at restoring hyperbolicity by incorporating a characteristic length scale in the governing equations.

The other difficulty of the problem is the multi-scale nature of the strain-localization phenomenon. Shear bands in metals are typically of the order of microns while the macro-specimen may be several meters in dimension. Hence, any meaningful discretization scheme, namely one which can accurately resolve the deformation field inside the shear band, must involve a huge amount of computational effort (e.g. [8])—the scale of which may exceed presently available resources for realistic engineering problems.

In the past [6], we have attempted to tackle the first of the above-mentioned problems by introducing viscosity in the constitutive equations. The resulting rate-dependent problem has a unique solution and yields mesh-invariant results provided the shear band be spanned by at least two elements. The width of the shear band is found to be approximatively equal to $10\,c\eta$, with $c$ a representative elastic wave speed and $\eta$ the relaxation time. Once the problem is rendered well-posed, we are however, still left with devising methods which can capture the structure of the strain field inside the shear band. In a second step, motivated by the work of Belytschko and co-workers [9–11], we proposed an enriched displacement procedure which attempts to incorporate additional degrees of freedom in patches

* Corresponding author.


*PII* S0045-7825(96)01068-7

covering the shear band inside selected elements [1]. This enables the element to resolve the shear band when the latter is several orders of magnitude smaller in dimension as compared to the characteristic size $h$ of the macro-element. The procedure was shown to be effective for elements whose characteristic size is more than 10 times the bandwidth $10c\eta$.

Another way to attempt to capture the details of the shear band is to refine the mesh at appropriate locations, so-called adaption procedure. For example, Ortiz and Quigley [12] and Belytschko and Tabarra [13] use refinement procedures while Peric et al. [14] and Zienkiewicz et al. [15] remesh the entire domain but increase the nodal density in a neighborhood of the band. There are qualitative arguments that support mesh refinement over remeshing for the simulation of strain-localization; in particular, the latter is more prone to smear the strongly localized mechanical information that characterizes shear-banding. While as stated earlier, adaption may prove to be stupendous for real-world problems, its usefulness in validating and comparing results from the enriched displacement procedure makes it worth pursuing. Further, it is possible that for practical engineering problems the method of choice will involve a combination of both procedures, namely adaption followed by displacement enrichment.

The paper is organized as follows. In Section 2, the governing equations and finite element formulation are briefly recalled. In Section 3, we explain the criteria used to select elements to be enriched. Section 4 describes briefly the mesh enrichment procedure. Section 5 deals with the various schemes to transfer the internal variables. The problems associated with selecting the appropriate time step for integrating the dynamical equations of motion are discussed in Section 6. Finite element analyses using the above ingredients are presented in Section 7 for several sample problems that involve different material properties and geometries. Comparisons between results obtained by adaption and enriched element procedures are presented and discussed.

## 2. Governing equations and FEM discretization

The strong form of the initial- and boundary-value problem is to obtain a displacement field which is continuous at each point $\boldsymbol{x}$ of the body $\Omega$ and at any time $t$ within the considered time interval $[0, T]$ and that satisfies:

$$\begin{aligned}
&\sigma_{ij,j} + \rho(b_i - \ddot{u}_i) = 0 && \text{in } \Omega \\
&u_i = u_i^d && \text{on } \partial\Omega_{u_i} \\
&\sigma_{ij} n_j = T_i^d && \text{on } \partial\Omega_{T_i} \\
&u_i(x, t=0) = u_{0i}(x) && \text{in } \Omega \\
&\dot{u}_i(x, t=0) = \dot{u}_{0i}(x) && \text{in } \Omega
\end{aligned} \tag{1}$$

where $\partial\Omega_{ui}$ and $\partial\Omega_{Ti}$ constitute a partition of the boundary $\partial\Omega$, the lower indices $i$ and $j$ vary between 1 and $n_{sd} = 2$, summation over repeated indices is assumed, the lower symbol '$j$' denotes partial derivative with respect to the space variable $x_j$ and a superposed dot ( $\dot{}$ ) denotes material time derivative. Also, $\rho$ is the mass density, $\boldsymbol{b}$ the body force per unit mass, $\boldsymbol{u}^d$ and $\boldsymbol{T}^d$ are the given displacement and traction, respectively, $\boldsymbol{n}$ is the unit outward normal to $\partial\Omega$ and $\boldsymbol{u}_0$ and $\dot{\boldsymbol{u}}_0$ are the given initial displacement and velocity. Implicit in the above is the fact that the stress $\boldsymbol{\sigma} = (\sigma_{ij})$ is obtained from the displacement and velocity by the constitutive equations.

In order to introduce the weak form associated with the strong form Eq. (1), let us define the space of admissible displacements $\mathcal{V}$ as

$$\mathcal{V}: \{\delta\boldsymbol{u} \in [\boldsymbol{H}^1(\Omega)], \delta\boldsymbol{u} = 0 \text{ on } \partial\Omega_u\}$$

The weak form is obtained by a componentwise multiplication of Eq. $(1)_1$ by an admissible but otherwise arbitrary displacement $\delta\boldsymbol{u}$ and integration by parts:

$$\int_\Omega \delta u_i\, \rho \ddot{u}_i\, \mathrm{d}\Omega + \int_\Omega \delta u_{(i,j)}\, \sigma_{ij}\, \mathrm{d}\Omega - \int_\Omega \delta u_i\, \rho b_i\, \mathrm{d}\Omega - \int_{\partial\Omega_T} \delta u_i\, T_i^d\, \mathrm{d}S = 0 \tag{2}$$

where $\delta u_{(i,j)}$ denotes the symmetric part of the gradient of the displacement $\delta \boldsymbol{u}$.

Within each element the displacement field is interpolated through the bilinear interpolation matrix $\boldsymbol{N}$:

$$\boldsymbol{u} = \boldsymbol{N}\boldsymbol{d} \tag{3}$$

where $\boldsymbol{d} = (d_i)$ denotes the nodal displacement vector. The displacement variation $\delta \boldsymbol{u}$ is interpolated through the same approximation functions as the trial displacement field $\boldsymbol{u}$. Thus

$$\delta \boldsymbol{u} = \boldsymbol{N}\, \delta \boldsymbol{d} \tag{4}$$

using similar notations for the trial displacement and displacement variation fields. The strain–vector $\boldsymbol{\epsilon} = [\varepsilon_{11}, \varepsilon_{22}, \varepsilon_{33}, \gamma_{12} = 2\varepsilon_{12}]^{\mathrm{T}}$ expressed componentwise in the Cartesian axes $(\boldsymbol{e}_1, \boldsymbol{e}_2, \boldsymbol{e}_3)$ can be obtained through the $\boldsymbol{B}$-matrix associated with the regular interpolation of the quadrilateral, or through the $\boldsymbol{B}$-bar modification of Hughes [16]:

$$\boldsymbol{\epsilon} = \boldsymbol{B}\boldsymbol{d} \tag{5}$$

with a similar expression for the strain variation vector $\delta \boldsymbol{\epsilon}$ due to Eq. (4).

Insertion of the discretization equations (Eqs. (3)–(5)) in the weak form Eq. (2) yields, due to the arbitrariness of the displacement variations $\delta \boldsymbol{d}$ and on assembling the element contributions:

$$\boldsymbol{M}\ddot{\boldsymbol{d}} = \boldsymbol{f}^{\mathrm{int}} = \boldsymbol{f}^{\mathrm{ext}} \tag{6}$$

where, a superposed $e$ denoting a quantity attached to element $e$, $e = 1$ to $N_{\mathrm{el}}$

$$\begin{aligned}
&\boldsymbol{M} = \boldsymbol{A}_{e=1}^{N\mathrm{el}} \boldsymbol{m}^e \\
&\boldsymbol{d} = \boldsymbol{A}_{e=1}^{N\mathrm{el}} \boldsymbol{d}^e \\
&\boldsymbol{f}^{\mathrm{int}} = \boldsymbol{A}_{e=1}^{N\mathrm{el}} \boldsymbol{f}^{e,\mathrm{int}}, \quad \boldsymbol{f}^{e,\mathrm{int}} = \int_{\Omega^e} \boldsymbol{B}^{\mathrm{T}} \boldsymbol{\sigma}\, \mathrm{d}\Omega \\
&\boldsymbol{f}^{\mathrm{ext}} = \boldsymbol{A}_{e=1}^{N\mathrm{el}} \boldsymbol{f}^{e,\mathrm{ext}}, \quad \boldsymbol{f}^{e,\mathrm{ext}} = \int_{\partial\Omega_T^e} \boldsymbol{N}^{\mathrm{T}} \boldsymbol{T}^d\, \mathrm{d}S + \int_{\Omega^e} \boldsymbol{N}^{\mathrm{T}} \rho(\boldsymbol{b} - \ddot{\boldsymbol{u}})\, \mathrm{d}\Omega
\end{aligned} \tag{7}$$

Actually, for efficiency, a diagonal mass matrix $\boldsymbol{M}$ is obtained through the row–sum technique (e.g. [16, p. 444]).

## 3. Enrichment criteria

Adaption schemes aim at defining an optimized mesh that minimizes a certain scalar quantity representative of the error between the exact and computed solutions. They require several ingredients, among which criteria to define locations where the mesh needs to refined and unrefined. Many error measures use elliptic estimates, as for example the strain–energy criterion of Zienkiewicz–Zhu [17]. However, such measures do not apply to strain-localization where the elliptic nature of the governing equations tends to be lost. Also, since a shear-band is a zone of intense plastic straining, the stress field is bound to be more or less uniform there; thus a criterion based on stress only is unlikely to be able to capture localization zones. These observations have prompted modifications of the Zienkiewicz–Zhu criterion. Peric et al. [14] use a criterion based on the rate of plastic work. Belytschko and Tabbara [13] suggest an error measure in terms of strains only: the idea being that the error will be large where the gradient of strain is large, which is indeed a mechanical manifestation of strain-localization. Other criteria use interpolation errors. The criterion of Diaz et al. [18] uses the second derivative of the displacement and so should be valuable to detect zones of high strain gradient; however it requires to

define the second derivative by interpolation over elements. Ortiz and Quigley [12] propose a resolution driven method where enrichment is performed for those elements which have a large velocity variation.

In our approach, we use three criteria to select the elements to be enriched. Two of them are resolution driven while the third criterion is directly related to the underlying material instability and uses the acoustic tensor. The three criteria selected as representative localization characteristics are assigned to the element center and they measure, respectively

- the velocity variations in the element [12]:

$$|\boldsymbol{v}|_{BV} = \max_i \left\{ \max_{a,b} |v_{ia} - v_{ib}| \right\} \tag{8}$$

where $v_{ia}$ are the nodal components of the velocity vector $\boldsymbol{v}$; $a$ and $b$ range over the nodes of the element and $i$ ranges over the degrees of freedom,

- the equivalent plastic strains:

$$\chi(t) = \int_0^t \|\dot{\epsilon}^{\mathrm{p}}(\tau)\| \, \mathrm{d}\tau \tag{9}$$

where $\dot{\epsilon}^{\mathrm{p}}$ is the plastic strain rate tensor,

- the trend to strain-localization through the ratio of the elastic and elastic-plastic acoustic tensors, $\boldsymbol{B}^{\mathrm{e}}$ and $\boldsymbol{B}^{\mathrm{ep}}$, respectively:

$$r = \min_{\boldsymbol{n}, \|\boldsymbol{n}\|=1} \frac{\det \boldsymbol{B}^{\mathrm{ep}}(\boldsymbol{n})}{\det \boldsymbol{B}^{\mathrm{e}}} \tag{10}$$

Thus, $r$ is equal to one for elastic unloading and zero at strain-localization.

It is argued in [19] that none of the above criteria can individually be taken as a sufficiently robust indicator for refinement. For example, the interpretation of contours of acoustic tensor ratio requires some care because this ratio depends on the plastic modulus which, in the numerical computations to be presented hereafter, is not varying monotonically. Besides, a criterion based only on the velocity variation criterion may not be satisfactory for the following qualitative reasons. Consider two elements, one small and the other much larger. It may happen that the velocity variation criterion be violated for the large element and not for the small one simply due to the geometry and irrespective of the loading content, e.g. for the same strain-rate. An additional problem with this criterion is its sensitivity to fluctuations in loading rate, especially under dynamic loading conditions. On the other hand, a criterion relying only on strains as in [15] or on plastic strains will certainly capture the shear-bands but our experience has shown that it is difficult to make it sufficiently sharp in order not to delay too much the refinement process.

The actual criterion adopted in this study is a combination of all of the above indicators. At the conclusion of every time step, the velocity variation $|\boldsymbol{v}|_{BV}$ and plastic strain $\chi$ for every element in the mesh are catenated and stored in separate vectors. Next, an elementary statistical analysis is performed. It involves sorting the components of the $|\boldsymbol{v}|_{BV}$ and $\chi$ vectors and computing their respective upper quartile values. The upper quartile value is that member of a set of real numbers, arranged in ascending order, which is exceeded in magnitude by only 25% of the members of the set. The upper quartile values of the $|\boldsymbol{v}|_{BV}$ and $\chi$ vectors, namely $|\tilde{\boldsymbol{v}}|_{BV}$ and $\tilde{\chi}$, are then used as localization delimiters. All elements whose $|\boldsymbol{v}|_{BV}$ and $\chi$ values exceed $|\tilde{\boldsymbol{v}}|_{BV}$ and $\tilde{\chi}$ and whose $r$ values lie below a prescribed minimum ratio, $\tilde{r}$, are assumed to be potential candidates for refinement. The value of $\tilde{r}$ is set at 0.01. A parameter analysis is presented in [19] to justify the definitions of the localization delimiters $|\tilde{\boldsymbol{v}}|_{BV}$, $\tilde{\chi}$ and $\tilde{r}$. Next, the set of candidate elements are grouped into clusters out of which bounded segments, the shear bands, are extracted through a least-squares analysis. The procedure is detailed in the above reference.

## 4. The enrichment procedure

In order to accurately resolve the structure of the shear band, it is essential that the level of discretization be such that the width of the band be spanned by at least two to three elements such that $h/10\,c\eta < 0.5$. In order to achieve this goal, we implement an adaptive refinement scheme which,

starting with an initial prescribed mesh, successively refines in sub-domains of interest. The procedure therefore belongs to the class of adaptive methods which rely on 'enrichment' to enhance resolution, rather than successive remeshings of the entire domain.

This approach is ideally suited to the localization phenomenon, because the interest is on the shear band which occupies a small fraction of the entire domain. Also, 'enrichment' as opposed to 'remeshing' has an extra advantage which makes it desirable for applications of this nature. In the quasi-static case, localization is triggered by material imperfections and occurs in those locations where imperfections exist. In dynamic problems, localization can initiate also in the absence of imperfections due to the boundary conditions and wave reflections. Now experiments suggest that subsequent material softening in the shear band may occur [20]. This necessitates that material properties be different in parts of the mesh—in particular, the band may have a different value of hardening modulus as compared to the surrounding back-bone material. Procedures which rely on splitting existing elements can easily incorporate this, since the material properties of the parent element are passed on to the successor elements. In case of remeshing however, it is not improbable that a refined element may comprise parts of two or more parent elements with different material properties. In that case assigning material properties to the refined element involves a measure ambiguity which is entirely avoided in the enrichment approach.

The enrichment approach used in this paper results in refined meshes consisting of four- and five-noded quadrilaterals. The advantage of using quadrilateral elements is that they can handle isochoric plastic deformations without the volumetric locking noticed in, for instance, three-noded triangular elements. Five-noded quadrilaterals act as transition elements and help in restricting mesh enrichment to the localization zone and its immediate neighborhood. In addition, the use of five-noded elements is necessitated on another count, since there exist domains which cannot be filled solely by four-noded quadrilaterals, for instance, domains having boundaries composed of an odd number of edges (cf. [21]).

The enrichment procedure is as follows. The elements to be enriched in the first place are those that are crossed by the shear bands, they will be referred to, by abuse of language, as 'localized' elements. They are divided into four successor elements. New nodes are added at the centroid and at the centers of all four sides. This allows for the Laplacian smoothing discussed in [22]. Thus, elements which are neighbours to the localized elements become five- and six-noded elements. Six-noded elements are transformed into 4 four-noded quadrilaterals or into transition macro-elements that contain 3 four-noded quadrilaterals. Some five-noded elements are transformed into 2 four-noded quadrilaterals. The key operations defining the procedure are displayed in Fig. 1.

In summary, four-noded quadrilaterals of the initial mesh are transformed into 2, 3 or 4 four-noded quadrilaterals or into five-noded quadrilaterals. In this way, the band and its immediate neighborhood are described by four-noded quadrilaterals only, five-noded elements which are thought to be less accurate are situated at some distance from the band and the transition macro-elements avoids unnecessary spreading of the refinement in the elastic unloading domain. This procedure is at variance with that of Belytschko and Tabarra [13] where both five- and six-noded elements are used.

The five-noded elements are used to ensure continuity of displacements and velocities across their boundaries. However, nodal values at the fifth node, say $C$, *are not solved for*; they are obtained by interpolation, using the bilinear shape functions, from the nodal values of the corner nodes along the corresponding side, say $A$ and $B$. Since for the present algorithm, the fifth node $C$ is always located at the mid-point of the line joining the corner nodes $A$ and $B$, this process is simplified and for a representative nodal variable $\phi$:

$$\phi_C = (\phi_A + \phi_B)/2 \tag{11}$$

For elements whose $C$ is a corner node, this also necessitates that their contributions to internal forces $f^{\text{int}}$ computed at node $C$ be added to the internal force contributions at nodes $A$ and $B$, respectively:

$$f_A^{\text{int}} = f_A^{\text{int}} + f_C^{\text{int}}/2 \tag{12}$$

$$f_B^{\text{int}} = f_B^{\text{int}} + f_C^{\text{int}}/2 \tag{13}$$

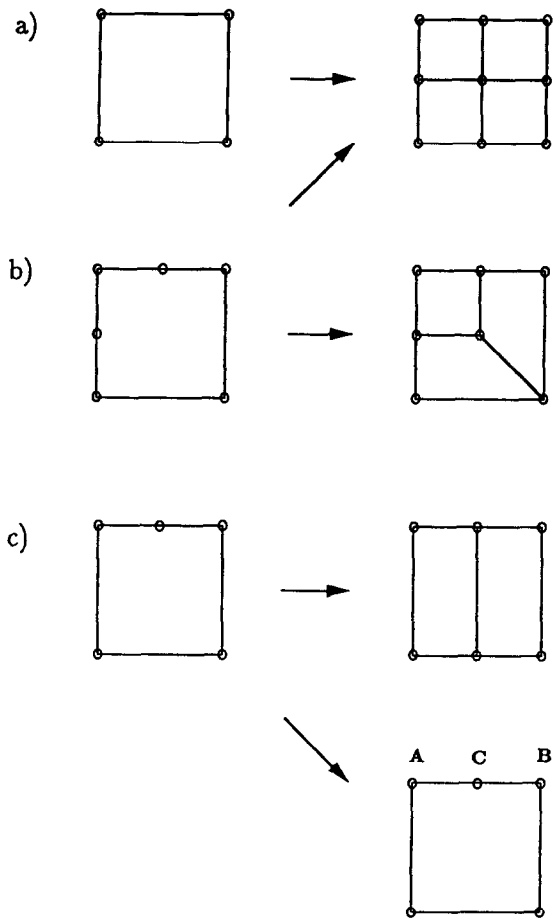


Fig. 1. Schematic of the enrichment procedure. 'Localized' four-noded splitted into 4 four-noded elements (a). Neighbors become five or six nodes which are processed as shown in (b) and (c).

Notice that the five-noded elements retain the characteristics of the four-noded bilinear quadrilateral, for example the estimates for the eigen-value bounds are the same as for the four-noded quadrilateral. The above procedure is suggested by Devloo et al. [23] for explicit computations.

Fig. 2 depicts an example of an original mesh and of the corresponding enriched mesh. Elements of the original mesh that are crossed by the shear band are divided into 4 four-noded quadrilaterals. The

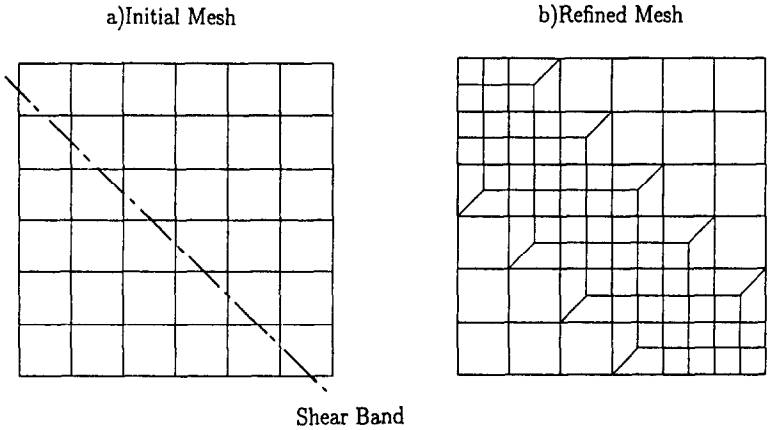


Fig. 2. A typical instance of the outcome of the refinement procedure illustrating the splittings shown in Figs. 1(a) and (b). Notice that the 'spill-over' is reduced to one row on each side of the 'localized' elements.

spill-over gives rise to six-noded elements which are all converted to transition macro-elements. This particular mesh does not give rise to any five-noded elements; examples of five-noded elements can be found in the meshes shown in Section 7.

## 5. Transfer of variables

### *5.1. A brief review*

Formulating adaptive finite element solutions for history-dependent materials involve several complexities. Unlike the elastic case, where the displacements and hence the stresses can be readily calculated on the refined mesh, the elasto-visco-plastic constitutive equations involve history-dependent variables which have to be appropriately transferred to the elements of the new mesh. This process is complicated by itself; in the case of localization, it is rendered more difficult owing to the need to preserve the localized character of the solution. During the process of transfer, the diffusion of internal variables, e.g. the plastic strains, should be limited; correlatively the velocity gradients must, as far as practicable, not get smeared over a part of the mesh exceeding the shear band. As we shall see, many of the proposed stress recovery schemes suffer from this defect which make them unsuitable for localization type applications.

In almost all recovery procedures, the internal variables of the pre-existing mesh are first subjected to a 'smoothing' operation before being transferred to the new mesh. This smoothing operation typically involves a nodal projection. For example, in global $L2$ projection procedures, the internal variables stored at the element stress points of the parent mesh are transferred to the nodes of the parent mesh by means of a least-squares minimization ([16, p. 227]).

After the internal variables have been transferred to the nodes of the parent mesh, using either the $L2$ projection procedure, or any of the alternatives mentioned in the next paragraph, the internal variables have to be recovered at the stress points of the refined mesh. To do this, every stress point of each element of the refined mesh has to be located in the parent mesh, that is, given the coordinates of a particular stress point, the element of the parent mesh in which it lies has to be identified. Once this is done, the state variables at the stress point can be obtained by interpolation, using the bilinear nodal shape functions, of the projected state variables stored at the nodes of the parent element. The process of identifying the element of the parent mesh, in which a particular stress point of the refined mesh lies, can be done by a sequential search through each element of the parent mesh until the appropriate parent element is identified, or alternatively, by using the Bucket Algorithm [29]. The Bucket Algorithm leads to a faster search, since it restricts the search to a smaller sub-domain of the parent mesh, identified through a prior pre-processing procedure. The above search, while inescapable during a remeshing procedure, may be avoided for a refinement procedure by storing an array containing the parents of newly created elements.

As an alternative to the $L2$ projection approach, Zienkiewicz and Zhu [17] develop a patch recovery procedure in which a single and continuous polynomial expansion of the function describing the internal variables is used on element patches surrounding the nodes at which recovery is desired. The expansion is made to fit locally the superconvergent points for the internal variables in a least-squares manner. Boundary nodes require special treatment. The procedure was subsequently modified by Wiberg et al. [24] and Blacker and Belytschko [25] to incorporate the equilibrium residual and the residual of the natural boundary conditions in the least-squares minimization functional. Blacker and Belytschko propose, in addition, a conjoint polynomial recovery procedure which is expected to improve the accuracy of the method.

As opposed to the above-mentioned smoothing procedures, Ortiz and Quigley [12] use a different approach. According to their procedure, the initial state fields are transferred to the quadrature points of the refined mesh by using an interpolation function which fits the values of the state variables at the quadrature points (stress points) of the parent mesh. This direct sampling procedure does not require nodal projection and therefore does not ensure continuity of the internal variables across the element boundaries. The authors report that they obtain convergent solutions with the six-noded triangular

element with three quadrature points per element. However, for four-noded bilinear quadrilaterals, extrapolation from the quadrature points gives rise to a jagged variation of the state fields across the elements, the refined mesh picks up the noise and the solution becomes corrupted. Since four-noded quadrilaterals are the elements of choice for the present procedure, the Ortiz–Quigley approach does not appear to be feasible for the purpose of this study.

We have implemented both the global $L2$-projection procedure as well as the patch recovery procedure of Zienkiewicz–Zhu both in its original and modified forms. Neither of the two procedures seem to be particularly effective. The global $L2$ projection and subsequent stress recovery, while they preserved the shear band in the refined mesh, were found to result in excessive smearing of the localized deformation. The Z–Z procedure however, even it its modified form, had a far more negative effect. The extent of the smearing was so severe that it was impossible to recover the shear band at its prior location before enrichment. The difficulties in devising a robust procedure to transfer the state variables during remeshing or refinement processes are indirectly illustrated in the papers by Peric et al. [14] and Zienkiewicz et al. [15]: in these two papers, computations are restarted from scratch at each adaption, thus avoiding totally the need for transfer.

### 5.2. *Modified L2 projection procedure*

As mentioned earlier, neither the $L2$ projection nor the Z–Z procedure seem to be particularly effective for localization calculations. Of the two, the $L2$ projection procedure appears more promising. In order to enhance its effectiveness, we propose some modifications. All the modifications are driven by the need to limit diffusion of localization characteristics into the non-localized region.

Thus, for all elements of the enriched mesh which do not map onto enriched elements in the parent mesh, the internal variables are directly transferred to the stress points of the enriched elements without performing the intermediate projection operations. For elements of the parent mesh which were not affected during the enrichment process, this is a natural choice. On the other hand, the successors of elements, which were not part of the shear band but still underwent some refinement due to the 'spill-over' effect, inherit exactly the state of their parent element: this is because the state variables are stored at a single stress point.

However, for all elements of the enriched mesh which are descendants of localized elements, the state variables are obtained through a least-squares procedure that involve all the elements of the parent mesh.

The above approach allows for the benefits of 'smoothing' for the localized elements thereby preventing the occurrence of the problems encountered by Ortiz and Quigley, namely those of 'noise' and consequent corruption of the localized solution. However, the state variables for elements outside the shear band are not subjected to 'smoothing'. This helps in preserving the localized character of the solution by limiting diffusion of shear band information.

### 5.3. *Transfer of primary variables*

The transfer of the primary variables—displacements, velocities and accelerations—present no difficulties. The nodal values of the parent mesh are transferred to the nodes of the new mesh using the nodal interpolation functions:

$$u_{ia,n+1} = \sum_b u_{ib,n} N_{b,n}(x_{a,n+1})$$

where $\boldsymbol{u} = (u_i)$ is a typical primary variable, $b$ denotes a node of the parent mesh $n$ and $a$ is a node of refined mesh $n + 1$.

## 6. Variable time stepping procedure

The global equations of motion (Eq. (6)) are integrated using an explicit predictor corrector scheme. Hence, the time step has to satisfy certain bounds in order to meet the stability conditions. For the trapezoidal integration used in this paper, the time step $\Delta t$ has to satisfy an inequality of the form

$$\Delta t \leq 2/\omega_{\max}$$

where $\omega_{\max}$ is the maximum eigenvalue of the generalized eigenproblem:

$$(\boldsymbol{K} - \omega \boldsymbol{M})\psi = 0$$

where $\boldsymbol{K}$ and $\boldsymbol{M}$ are the tangent stiffness and mass matrices, respectively. Also, as mentioned in Section 2, for numerical efficiency a lumped mass matrix is used. It is known that the maximum eigenvalue of the entire mesh cannot exceed the maximum eigenvalue of any of its elements. Thus, $\omega_{\max}$ is chosen to be the maximum among all the eigenvalues of each of the individual elements. Following the enrichment procedure described in Section 4, it is expected that the mesh will comprise quadrilaterals which may not necessarily be rectangular in shape. While the expression for the eigenvalue bounds for rectangular elements is well known, for quadrilaterals with arbitrary geometric configurations, bounds have been obtained only for four-noded elements [26]. In addition, these bounds are limited to one point quadrature and a lumped mass matrix. The bound on $\omega_{\max}$ is given by

$$\omega_{\max} \leq c g^{1/2}$$

where $c$ is the elastic longitudinal speed and

$$g = \frac{4}{A^2} \sum_{i=1}^{2} \sum_{a=1}^{4} B_{ia} B_{ia}\,,$$

$$B_{ia} = \begin{bmatrix} (y_2 - y_4) & (y_3 - y_1) & (y_4 - y_2) & (y_1 - y_3) \\ (x_4 - x_2) & (x_1 - x_3) & (x_2 - x_4) & (x_3 - x_1) \end{bmatrix} \tag{14}$$

where $x_a$ and $y_a$ are the coordinates of node $a$ and $A$ is the area of the element. In the present work, though uniform reduced one point quadrature was not used in the calculation of internal forces, the above estimate of the bound was not observed to give rise to instability even after a large time interval (see Section 7.3).

## 7. Numerical examples

In order to illustrate the computational procedure described in the preceding sections, the simplest elastic-plastic solid is chosen, namely a von Mises associative material with isotropic hardening. The details of the yield function and hardening rule used have been described in [6]. The size $k$ of the yield surface in deviatoric stress–space is a function of the equivalent plastic strain $\chi$. In the applications to be presented hereafter, $k$ is taken to be a piecewise-linear function of $\chi$:

$$k(\chi) = \begin{cases} k_0 + H_1 \chi & \text{if } \chi \leq \chi_1 \\ k(\chi_1) & \text{if } \chi \geq \chi_1 \end{cases} \tag{15}$$

where $k_0$, $H_1$ and $\chi_1$ are material parameters constrained to satisfy the condition $k(\chi_1) > 0$. Therefore, the plastic modulus is equal to $H_1$ for $\chi \leq \chi_1$ and is zero for $\chi > \chi_1$. Values for the material parameters have been included in Table 1 except for the plastic modulus and the relaxation time which will be specified for each problem analyzed.

Visco-plasticity is introduced as a regularization procedure (see e.g. [6]). The regularization makes use of a new parameter $\eta > 0$ called relaxation time. The equations of motion remain hyperbolic and it is possible to simulate numerically the development of shear-bands with finite thickness: indeed, the

Table 1
Standard material parameters

| |
|---|
| Mass density $\rho = 2000\ \text{kg/m}^3$ |
| Lamé coefficient $\lambda = 0$ |
| Elastic shear modulus $\mu = 320\ \text{MPa}$ |
| Initial yield strength $k_0 = \sqrt{2}\ \text{MPa}$ |
| Reference plastic strain $\chi_1 = 2\%$ |

governing equations involve the product $c\eta$ of the elastic wave-speed by the relaxation time which acts as a length-scale.

The typical initial- and boundary-value problems analyzed are as follows. A homogeneous elasto-visco-plastic rectangular specimen with sides $2L_1$ and $2L_2$ is subjected along its top and bottom boundaries to a uniform axial tensile velocity jump $\Delta v\, H(t)$, $H(t)$ being the Heaviside step function, while the lateral sides remain traction-free. The solid is initially stress-free and the magnitude of the velocity jump $\Delta v = 1.4$ m/s is chosen to ensure that plastic loading initiates along the symmetry line when the elastic waves coming from the top and bottom boundaries collide, i.e. $\frac{1}{2}\Delta v_0 < \Delta v < \Delta v_0$ with $\Delta v_0 = \sqrt{\frac{3}{2}} k_0/\rho c$, ([27, Eq. (21)]). Because of the symmetry conditions, only the upper right quarter of the specimen is considered. Actually, most of problems analyzed are for a square specimen of side $2L = 0.12$ m. The effects of geometry on the shear band pattern will be studied on specimens of aspect ratios 2 and 4.

The strain-localization scenario for the plastic moduli used in this paper starts as follows (see however [19] for the effects of the plastic modulus on the shear band pattern). Strains begin to concentrate at the free boundary on the symmetry line just after the arrival of the elastic waves coming from the top and bottom horizontal sides of the specimen. Then the strain concentration moves upwards almost along the diagonal of the specimen while the shear-band develops behind.

### 7.1. *Validation of the adaptive meshing procedure*

The first set of results are for hardening modulus $H_1 = -60$ MPa and relaxation time $\eta = 6.25 \times 10^{-7}$ s. The initial mesh comprises 36 equal-sized square elements spanning a quarter of the problem domain. For this mesh, $h/10\, c\eta = 4$, where $\eta$ is the characteristic size of the element. The mesh is successively refined, thereby yielding smaller values of $h/10\, c\eta$. The transition from one stage of refinement to the next is made once there are a sufficient number of elements satisfying the combined localization criterion described in [19]. For the number of elements to be sufficient, the shear band must be fully formed; tests to ascertain this were implemented and have been presented in the above reference. In order to check that the transfer procedure described earlier in Section 5 is satisfactory, we examine the transition for the mesh with $h/10\, c\eta = 1$ to a mesh with a higher level of discretization ($h/10\, c\eta = 0.5$). Comparison of the deformed shape and velocity fields shown in Fig. 3 at steps 44 and 45 corresponding to axial strains equal to 1.325% and 1.3285%, respectively, indicates that the nodal variables have been correctly transferred between the two meshes; the same observation holds for the equivalent plastic strains shown in Fig. 4.

The computed results for the same final axial strain of 5% at the same time T are shown in Figs. 6–9. Fig. 6 shows the deformed meshes and velocity fields. Fig. 7(a) shows the shear band width for several mesh refinements including each of the 4 meshes of Fig. 6 and Fig. 7(b) the maximum plastic strains in the shear band. The plastic strain profiles across the shear band are shown in Fig. 8 and Fig. 9 shows the corresponding force measured on the upper platens versus displacement curves.

As mentioned in Section 4, experimental results suggest that differences in material properties are likely to grow between the shear band and the surrounding material: the large strains that develop in the band may trigger various physical phenomena that imply degradation of the mechanical properties. Here, we account for that observation in a rather crude way by assigning additional softening to the 'localized' elements of size smaller than $10\, c\eta$. For illustration, the elements with reduced hardening modulus have been marked in Fig. 5 for the refined mesh with $h/10\, c\eta = 1$. It is important to emphasize that the change of material properties is done only *after* the localization pattern has clearly emerged in the enriched mesh and *only* in elements which belong to the putative band. For the present problem, in all such elements $H_1$ is reduced to $-70$ MPa. Comparing the deformed mesh for $h/10\, c\eta = 2$ (Fig. 6(a)) with the deformed mesh for $h/10\, c\eta = 1$ (Fig. 6(b)), it is clear that in this case mesh refinement leads to narrowing of the shear band as depicted in the convergence plot shown in Fig. 7(a): while the shearing in Fig. 6(a) is concentrated over one element of the $h = 20\, c\eta$ mesh, in Fig. 6(b) it is still over one element of the $h = 10\, c\eta$ mesh. Two further refinements are performed corresponding to $h/10\, c\eta = 0.5$ and $h/10\, c\eta = 0.25$. Now in both cases, the shear band is spread over $10\, c\eta$. This behavior is in

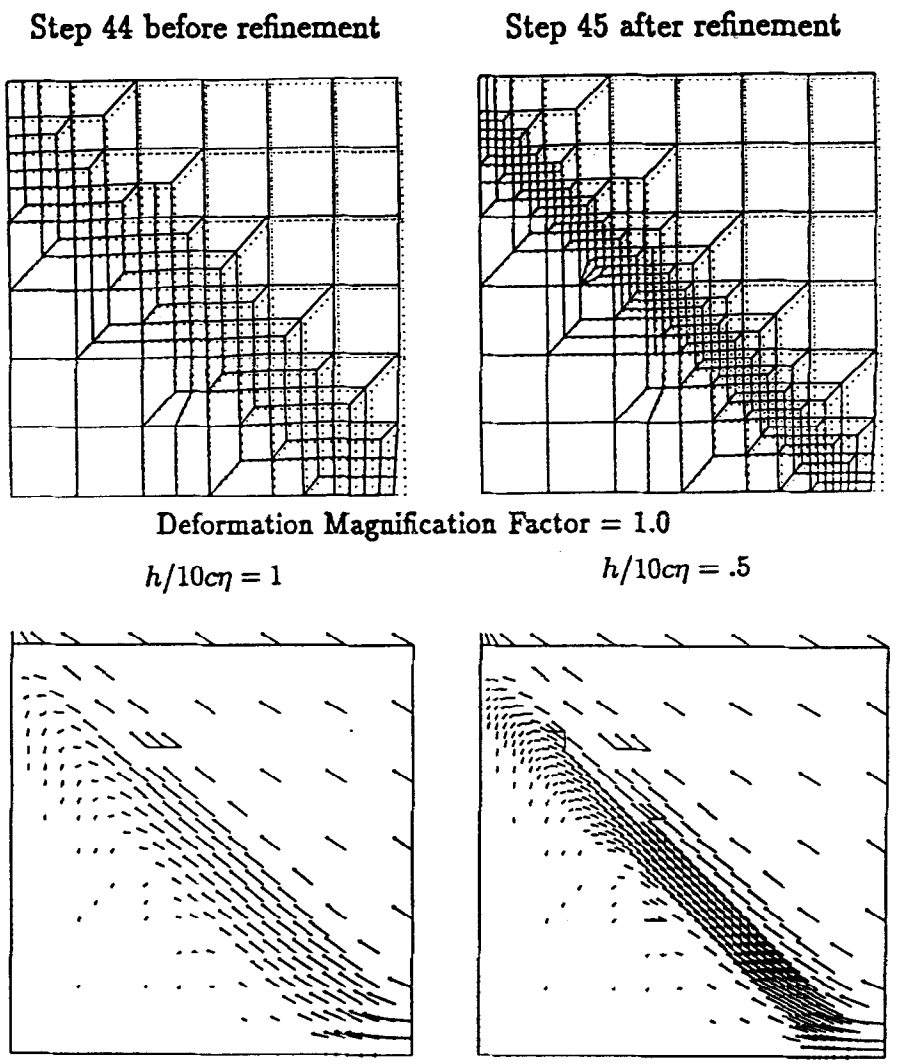


Fig. 3. Transfer of nodal variables. (a) Deformed mesh; (b) velocity field for mesh with $h/10\,c\eta = 1$ at step 44 before refinement; (c) deformed mesh; (d) velocity field for mesh with $h/10\,c\eta = 0.5$ at step 45 after refinement ($H_1 = -60$ MPa, $\eta = 6.25 \times 10^{-7}$ s).

remarkable contrast to the transition from the $h/10\,c\eta = 2$ to the $h/10\,c\eta = 1$ meshes, when mesh refinement led to a clear sharpening.

To clearly depict the convergence of the solution with refinement, the shear band widths and maximum plastic strains are plotted for the successive refines meshes in Fig. 7. To avoid ambiguity, the shear band width for a particular mesh is defined as the width of the plastic strain profile at the location at which 15% of the maximum value of the plastic strain for that mesh is attained. For instance, for the mesh with $h/10\,c\eta = 1$, since the maximum plastic shear strain at time T is 57% the shear band is measured at the location where the plastic strain is 8.5%. Fig. 7(a) clearly shows that the shear band width narrows with refinement and ultimately converges. The curves for the maximum plastic strain in Fig. 7(b) and the strain profiles in Fig. 8 also replicate this convergence behavior. The converged band thickness is found to be about $15\,c\eta$, which closely approximates the expected value of $10\,c\eta$. The convergence plots confirm our previous remarks that the details of the shear band characteristics are captured with sufficient accuracy as soon as the band spans over two elements.

Also, the force versus displacement curves are compared for the enriched meshes (Fig. 9). Comparing the curves for the various levels of enrichment leads us to conclude that the effect of the additional softening predominates. For higher values of $h/10\,c\eta$, the additional softening, since it is spread over a distance $h$, has a more marked effect. Hence, higher values of $h/10\,c\eta$ correspond to

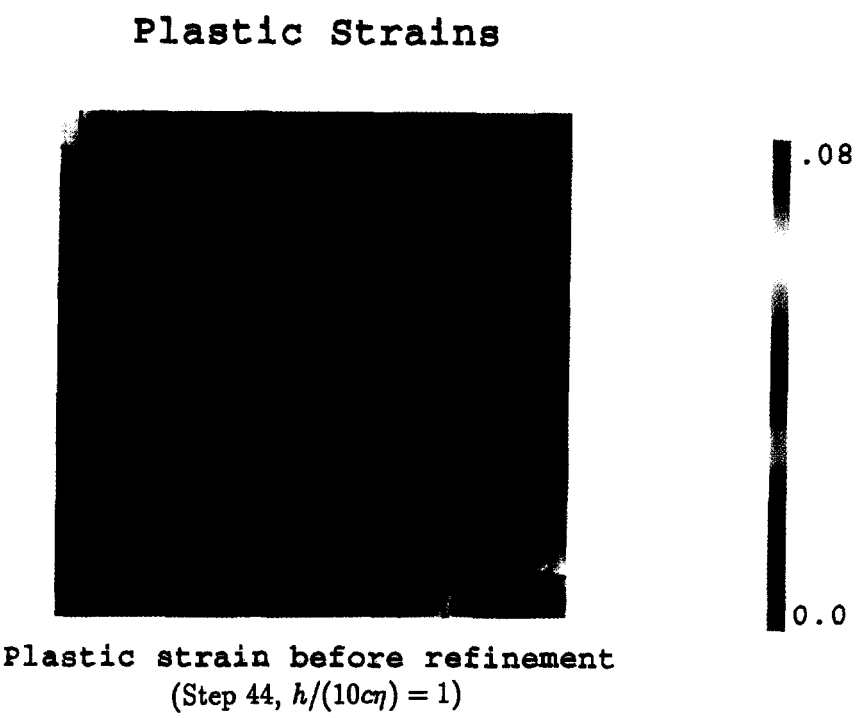


Fig. 4. Transfer of internal variables. (a) Plastic strains for mesh with $h/10\,c\eta = 1$ at step 44 before refinement; (b) plastic strains for mesh with $h/10\,c\eta = 0.5$ at step 45 after refinement ($H_1 = -60$ MPa, $\eta = 6.25 \times 10^{-7}$ s).

force–displacement curves with deeper troughs. It is noted however that as the mesh is refined, the force–displacement curves approach each other, thereby exhibiting convergence of the shear band solution. For instance, the troughs for $h/10\,c\eta = 0.5$ and $h/10\,c\eta = 0.25$ are practically the same. From Fig. 9, it seems that the force–displacement curves are not sensitive to the micro-structural details of the strain localization phenomena; they appear to be more responsive to changes in properties in the macro-level constitutive equations.

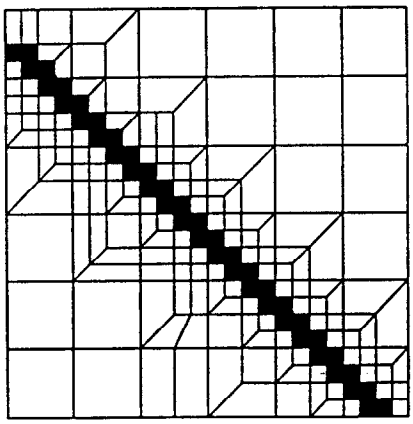

Fig. 5. Changes in material properties after localization: the plastic modulus in 'localized' elements is assumed to simulate mechanical degradation.

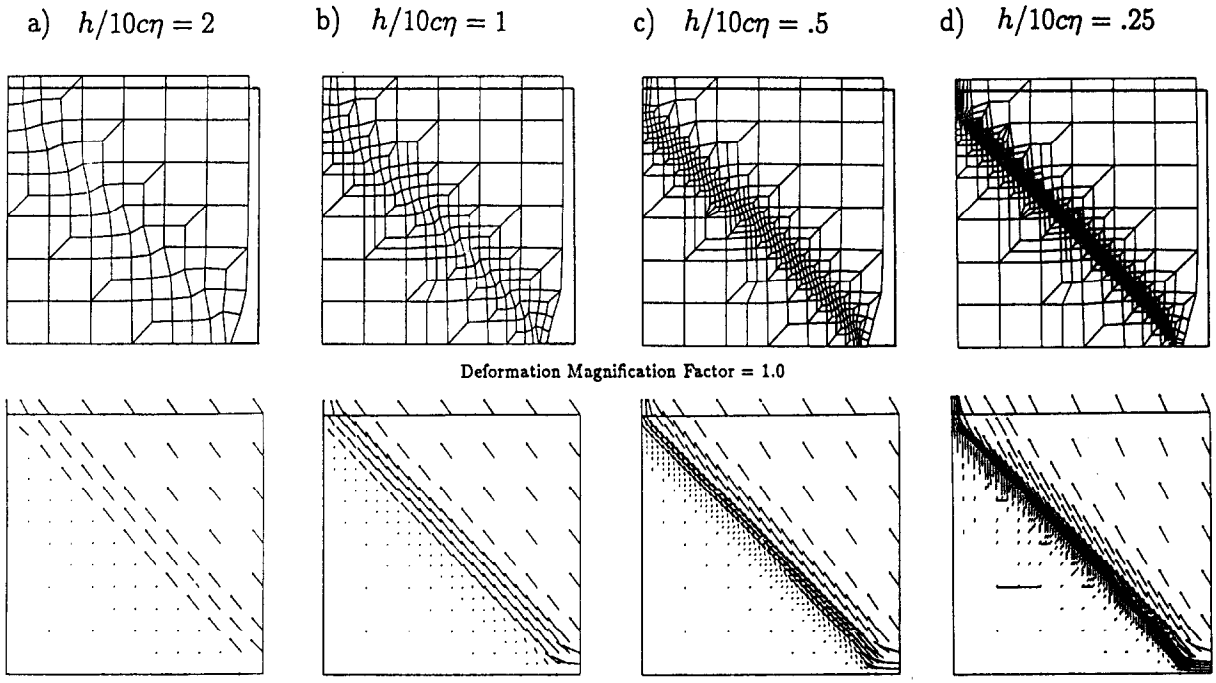


Fig. 6. Deformed meshes and velocity fields at the same axial strain of 5% for various meshes: $h/10\,c\eta = 2,\ 1,\ 0.5,\ 0.25$ ($H_1 = -60$ MPa, $-70$ MPa, $\eta = 6.25 \times 10^{-7}$ s).

## 7.2. Comparison with enriched displacement procedure

### 7.2.1. Influence of the constitutive equations

Reducing the value of the relaxation time $\eta$ results in the regularized elasto-(visco)-plastic solid approximating the elasto-plastic backbone material more closely. Thus, reducing $\eta$ leads to narrowing of the shear band, and allows us to compare the results of the adaptive meshing procedure with solutions obtained using the enriched displacement approach (cf. discussion at the end of Section 7.2.2). We solve the same problem as in the last example with $H_1 = -40$ MPa and the relaxation coefficient is reduced to nearly one fifth of its previous value, namely $\eta = 1.5 \times 10^{-7}$ s. The problem is solved for seven meshes, $h/10\,c\eta = 16.7,\ 8.35,\ 4.18,\ 2.09,\ 1.05,\ 0.525,\ 0.263$. The enriched meshes are depicted in Fig. 10. Additional softening of $H_1 = -50$ MPa is introduced in all successors of the localized elements over the width $10\,c\eta$ when $h/10\,c\eta \leq 1$. Variations of the shear band width and maximum plastic strain

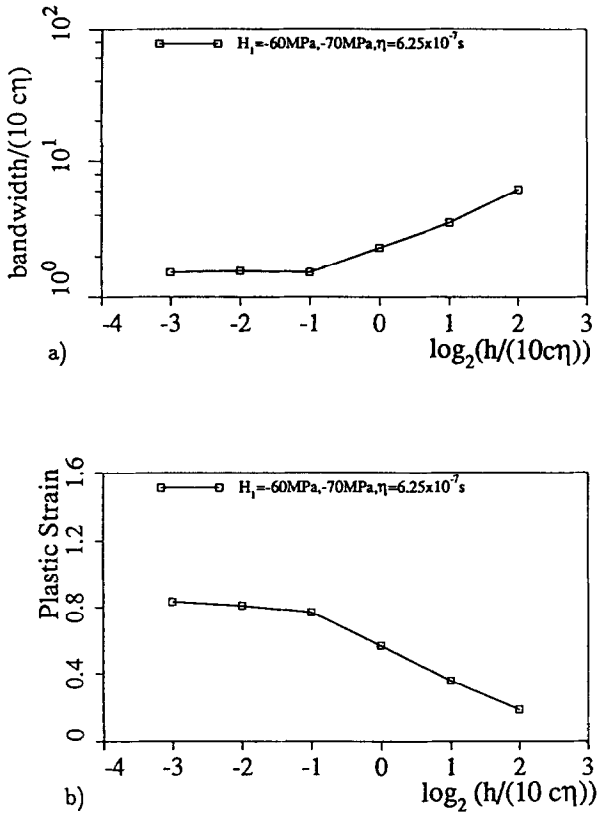


Fig. 7. Convergence of shear band widths (a) and maximum plastic strains (b) with refinement for an axial strain equal to 5% ($H_1 = -60$ MPa, $-70$ MPa, $\eta = 6.25 \times 10^{-7}$ s).

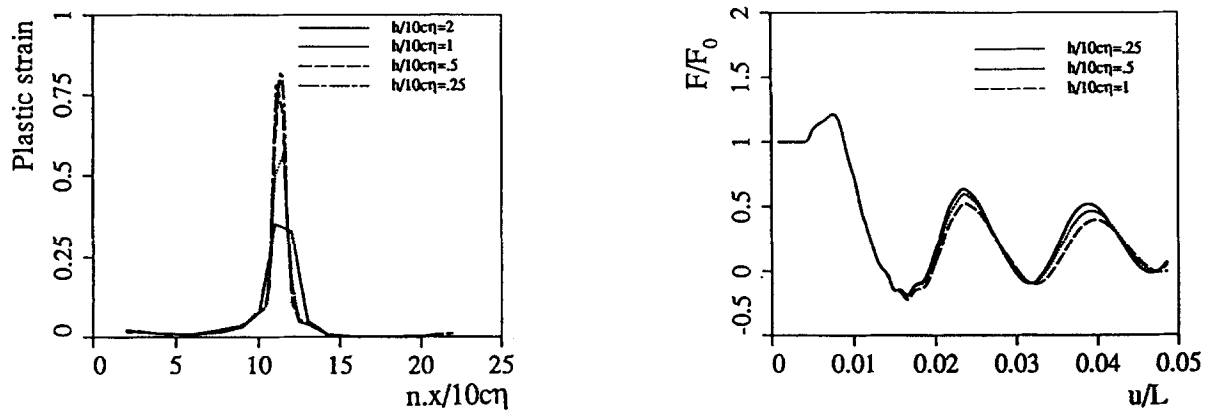


Fig. 8. Plastic strain profiles at the same axial strain of 5% for various meshes: $h/10c\eta = 2$, 1, 0.5 and 0.25 ($H_1 = -60$ MPa, $-70$ MPa, $\eta = 6.25 \times 10^{-7}$ s).

Fig. 9. Normalized force–displacement curves for various meshes: $h/10c\eta = 2$, 1, 0.5 and 0.25. $F_0$ is the impact force ($H_1 = -60$ MPa, $-70$ MPa, $\eta = 6.25 \times 10^{-7}$ s).

with increasing refinement are depicted in Fig. 11(a) and (b). Again, the plastic strains increase and shear bands narrow as the mesh is refined. Both shear band width and plastic strain converge with refinement. In order to compare the adaptive meshing solutions with the results of the enriched displacement procedure, we solve, using the enriched displacement procedure, the same problem for the $6 \times 6$ mesh; for $\eta = 1.5 \times 10^{-7}$ s this results in $h/10c\eta = 16.67$. Comparing the adaptive meshing solutions with the plastic strain profile obtained from the enriched displacement procedure, we note

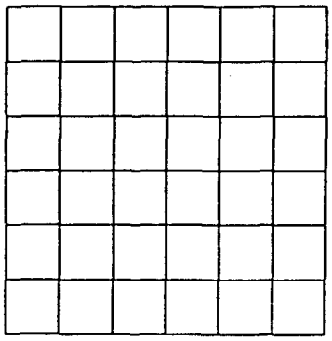

Initial Mesh $h/10c\eta = 16.8$

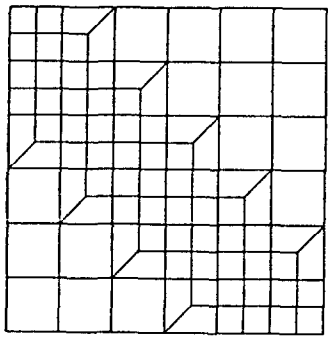

$h/10c\eta = 8.4$

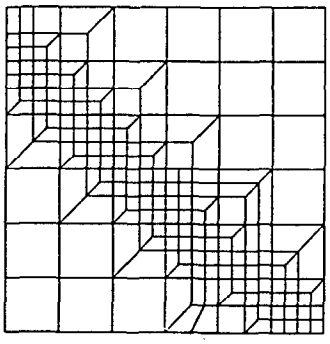

$h/10c\eta = 4.2$

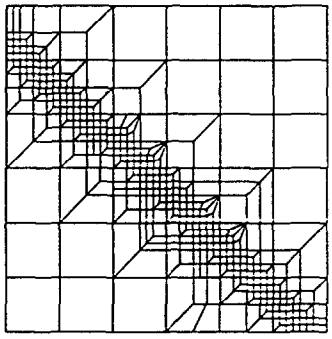

$h/10c\eta = 2.1$

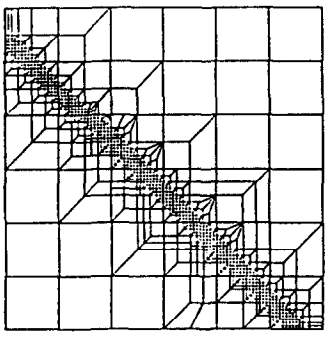

$h/10c\eta = 1.05$

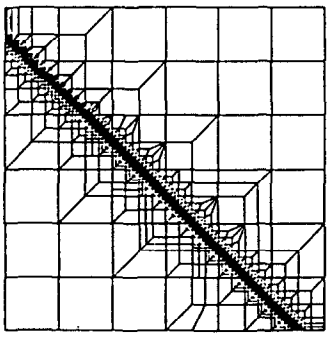

$h/10c\eta = .525$

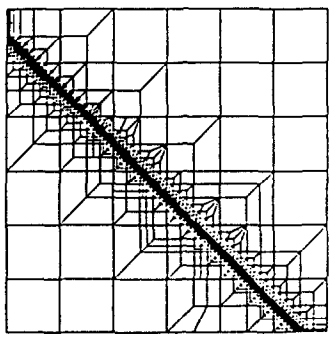

$h/10c\eta = .2625$

Fig. 10. Undeformed enriched meshes for $h/10\,c\eta = 16.8, 8.4, 4.2, 2.1, 1.05, 0.525, 0.2625$ ($H_1 = -40$ MPa, $-50$ MPa, $\eta = 1.5 \times 10^{-7}$ s).

that, while the width of the band for the highest level of mesh refinement ($h/10\,c\eta = 0.263$) is about $12\,c\eta$, the enriched displacement solution predicts a bandwidth of $9\,c\eta$ (Fig. 11(a)). The magnitude of the plastic strain in the patch is also comparable to that obtained from adaptive meshing (Fig. 11(b)).

To verify the above conclusions, we solve the problem for the same value of relaxation time but with hardening modulus $H_1 = -60$ MPa. The problem is again solved for seven meshes, with $h/10\,c\eta = 16.7$, 8.35, 4.18, 2.09, 1.05, 0.525, 0.263 as before. Additional softening ($H_1 = -70$ MPa) in the putative localized elements enhances the localization pattern. The variations of the band thickness and maximum plastic strain with increasing refinement are again depicted in Fig. 11(a) and (b). As in the last example both shear bands and plastic strains converge with refinement. The band width at the

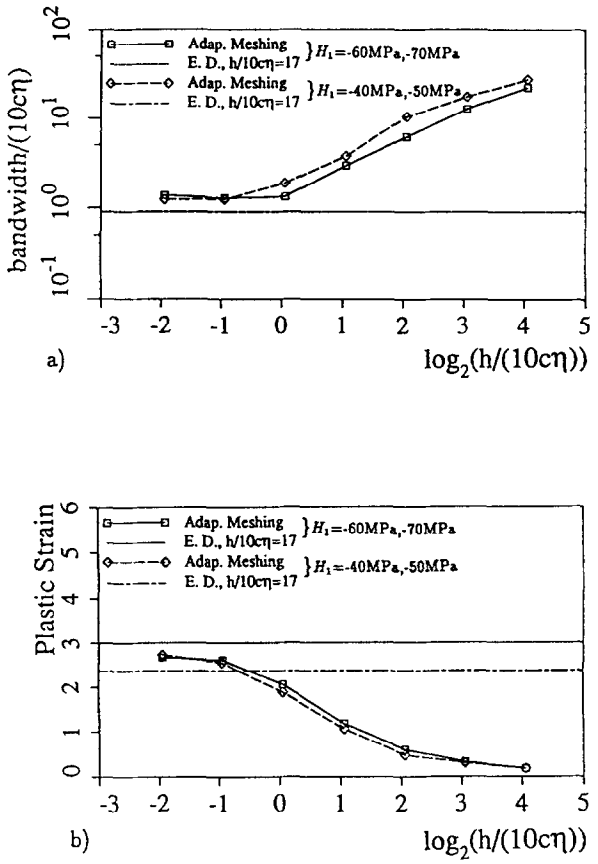


Fig. 11. Convergence of shear band widths (a) and maximum plastic strains (b) with refinement for two hardening moduli and for both adaptive meshing and enriched displacement procedures. Axial strain = 5%, $\eta = 1.5 \times 10^{-7}$ s.

highest level of refinement is found to be $13\,c\eta$. In this case also the patch resolves the band width to the neighborhood of its expected value, around $9\,c\eta$, while the maximum plastic strain is of the same order as that obtained from the adaptive meshing procedure.

### 7.2.2. *Influence of the ratio element size/bandwidth*

To test the bounds of the domain in which both procedures are effective, we solve three more problems with relaxation times $\eta = 1.25 \times 10^{-7}$ s, $\eta = 1.75 \times 10^{-7}$ s and $\eta = 2.5 \times 10^{-7}$ s. All three problems have $H_1 = -60$ MPa for the underlying material and $H_1 = -70$ MPa in the shear band and are each solved for six levels of mesh refinement. For the problem with $\eta = 1.25 \times 10^{-7}$ s, the meshes vary from $h/10\,c\eta = 20.0$ to $h/10\,c\eta = 0.31$, while, for $\eta = 1.75 \times 10^{-7}$ s, the meshes vary from $h/10\,c\eta = 14.29$ to $h/10\,c\eta = 0.22$, and for the problem with $\eta = 2.5 \times 10^{-7}$ s, the meshes range between $h/10\,c\eta = 10$ to $h/10\,c\eta = 0.156$. The enriched displacement solution in all cases is for the $6 \times 6$ mesh; for $\eta = 1.25 \times 10^{-7}$ s this results in $h/10\,c\eta = 20$, for $\eta = 1.75 \times 10^{-7}$ s, $h/10\,c\eta = 14.29$ while for $\eta = 2.5 \times 10^{-7}$ s the corresponding value of $h/10\,c\eta$ is 10. The variations of maximum plastic strain and band thickness with increasing refinement are depicted in Fig. 12. Both shear bands and plastic strains converge with refinement. The results from mesh refinement and enriched displacement procedures are quite similar. However, for $\eta = 2.5 \times 10^{-7}$ s, while the maximum plastic strain is of the same order for both procedures, the enriched displacement solution yields a much smaller value of the band width: approximately $6\,c\eta$. This is because we have now entered the region where the enriched displacement

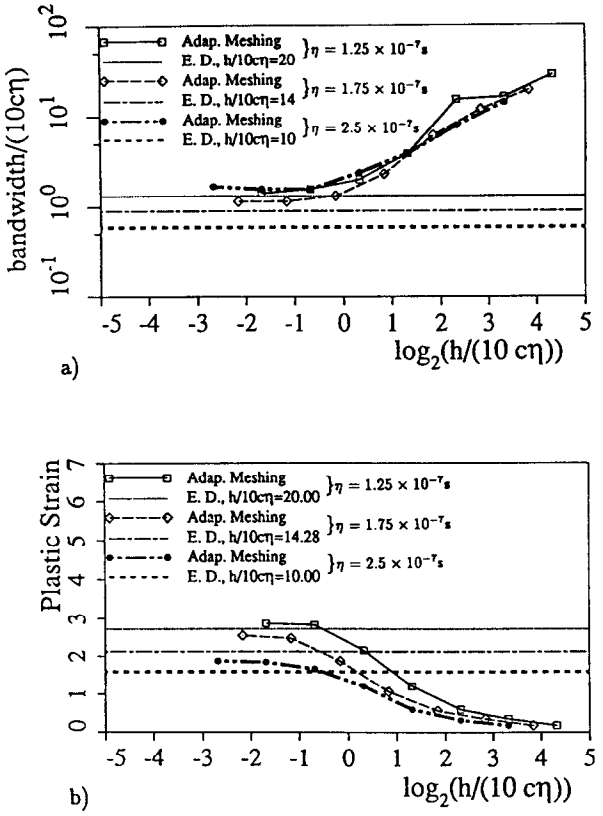


Fig. 12. Convergence of shear band widths (a) and maximum plastic strains (b) with refinement for three relaxation times and for both adaptive meshing and enriched displacement procedures. Axial strain = 5%, $H = -60$ MPa, $-70$ MPa.

procedure starts losing its validity. For $h/10\,c\eta$ larger than 10, i.e. for cases where the putative shear band width is at least one order of magnitude smaller than the characteristic size of the element, the enriched displacement procedure is found to perform well. However, for $h/10\,c\eta$ equal to and smaller than this value, we have conjectured that the range in which it can be safely used has been exceeded as explained in [1], Section 3.8; in such cases, the adaptive meshing procedure should be used to resolve the structure of the shear band.

### 7.3. *Temporal stability*

To test whether the shear band widths differ significantly from the converged solution at time T corresponding to an axial strain of 5%, the same problem as in Section 7.1 was solved for times greater than T for the mesh with $h = 2.5\,c\eta$. As mentioned in Section 7.1, the converged shear band width at time T for this problem was found to be about $15\,c\eta$, hence we expect the band to be spanned by more than six elements. The loading process is continued up to time 2.25 T. Time 2.25 T corresponds to 25 to and fro traversals of the problem domain by the impacting wave. As Fig. 13(a) shows, the shear band widths vary little with time, the minor fluctuations in their values can be attributed to measurement errors: this is expected since, due to the visco-plastic regularization [6], the shear band width is set by the internal length scale parameter $c\eta$. The same conclusion can be drawn from the strain profiles shown in Fig. 13(c). The plot of the maximum plastic strains in Fig. 13(b) shows an almost linear variation with time: this behavior is to be contrasted with the results reported in [28], wherein the plastic strains in the band are found to increase exponentially with time.

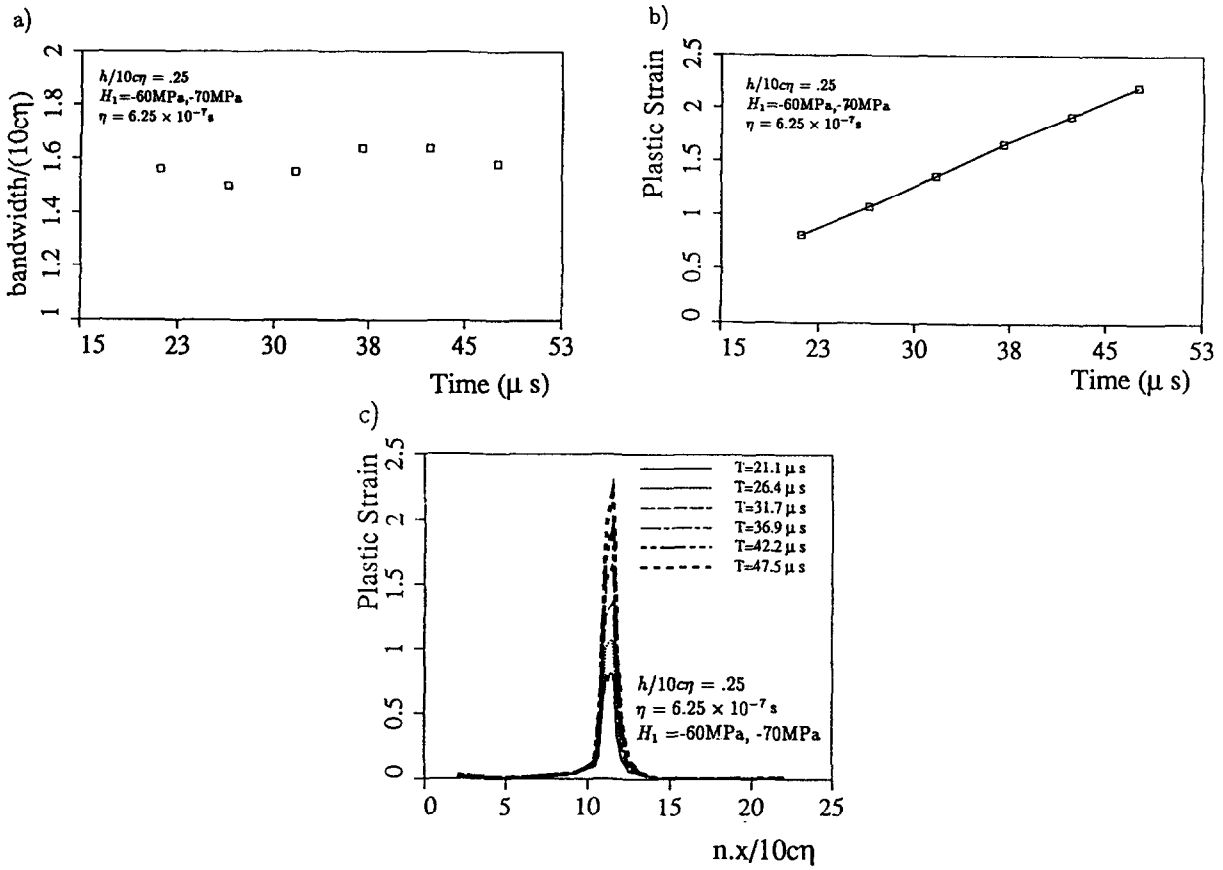


Fig. 13. During the deformation process, the shear band width (a) keeps a constant value while (b) plastic strain increases linearly; (c) plastic strain profiles at various times ($h/10c\eta = 0.25$, $H_1 = -60$ MPa, $-70$ MPa, $\eta = 6.25 \times 10^{-7}$ s).

### 7.4. *Examples with more than one band*

The next two sets of results are for problem geometries which give rise to more than one shear band. For both sets of results $H_1 = -30$ MPa and $\eta = 6.25 \times 10^{-7}$ s. Degradation of material properties is simulated by a plastic modulus $H_1 = -45$ MPa in the localized elements.

For the first specimen with sides $2L_1 = 0.12$ m and $2L_2 = 0.24$ m, the first shear band is initiated at the free boundary on the symmetry line, just after the arrival of the elastic waves coming from the top and bottom horizontal sides. Once this shear band reaches the center line, it is reflected and gives rise to another band at approximately right angle to it. The deformed meshes and velocity fields for two successive refined meshes are shown in Fig. 14, along with those for the initial mesh. Starting with $h/10c\eta = 2$ successive refinements yield $h/10c\eta = 1$ and $h/10c\eta = 0.5$, respectively.

The second specimen is thin and wide with sides $2L_1 = 0.48$ m and $2L_2 = 0.12$ m. The first shear band is again initiated on the symmetry line on the bottom right-hand corner of the free boundary. On propagation it is reflected at the top boundary and gives rise to a second band approximately at right angle to the first band. This process continues along the entire width of the specimen ultimately giving rise to four shear bands. Deformed meshes and velocity fields for the initial mesh as well as for two successive refinements are shown in Fig. 15. Mesh refinement helps resolve the shear bands. This is found to be particularly true for the third and fourth bands in the specimen. This same problem has been solved for the mesh $h/10c\eta = 2$ with the enriched displacement procedure (Fig. 10 in [19]): all four bands formed at the same location as in adaptive meshing here but the localization pattern is more diffuse for the third and fourth bands.

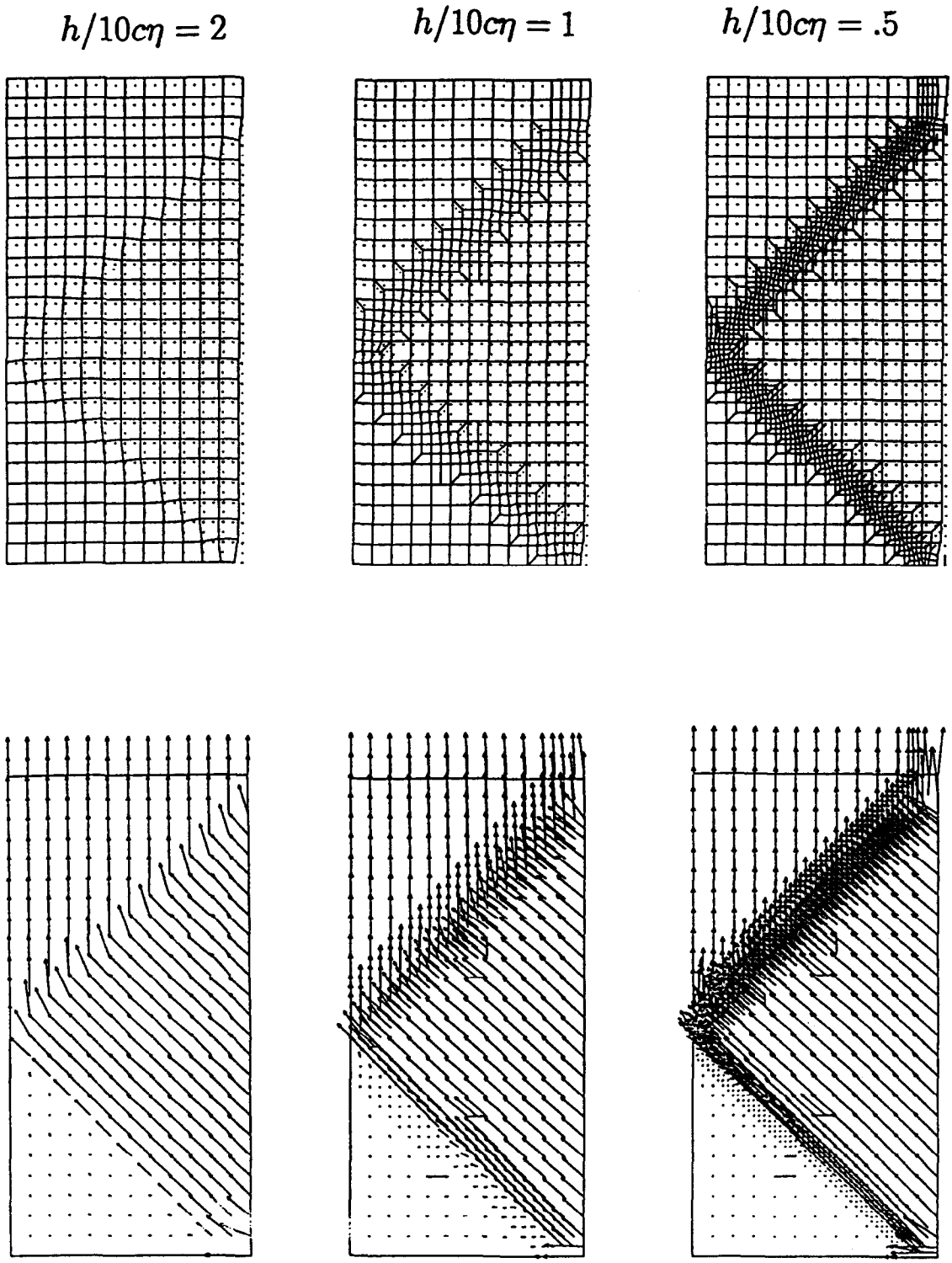


Fig. 14. In a slender specimen, the localization pattern exhibits two bands: the second one is due to the reflection of the lower one along the vertical symmetry axis. Deformed meshes and velocity fields for $h/10\,c\eta = 2$, 1 and 0.5 and an axial strain equal to 3.08% ($H_1 = -30$ MPa, $-45$ MPa, $\eta = 6.25 \times 10^{-7}$ s).

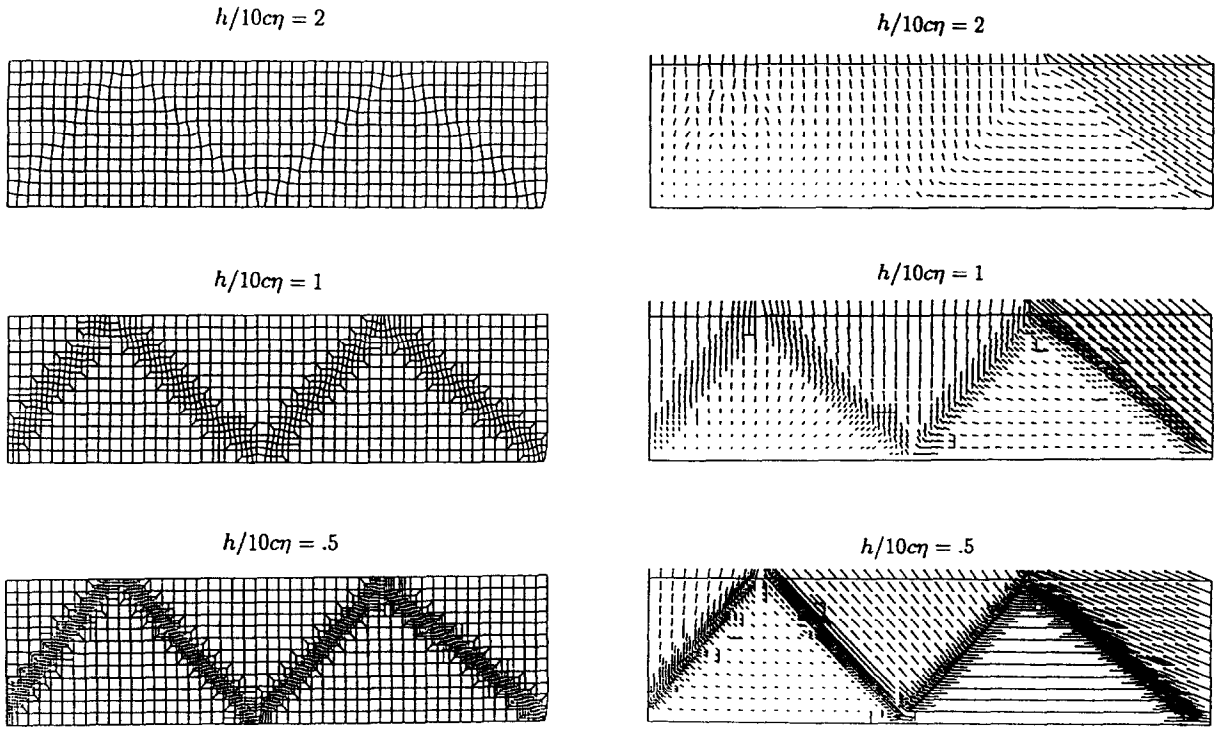


Fig. 15. For a thin and wide specimen, the band pattern progresses towards the interior of the solid by successive reflections, on the upper boundary and horizontal symmetry axis, of the right shear band emanating from the free boundary. Deformed meshes and velocity fields for $h/10c\eta = 2$, 1 and 0.5 and an axial strain equal to 6.57% ($H_1 = -30$ MPa, $-45$ MPa, $\eta = 6.25 \times 10^{-7}$ s).

## 8. Concluding remarks

The dynamic strain localization problem is solved using a mesh enrichment approach. The aim is to resolve the shear band structure through successive refinements of the finite element mesh. A refinement criterion using three localization characteristics is employed. Elements used are four- and five-noded quadrilaterals. A modified procedure for transferring internal variables is implemented. The results yield consistent and stable solutions. In particular, the shear band width and maximum plastic strain in the band are found to converge to stable values with refinement.

It should be emphasized that localization in the above problems is not triggered by the presence of an imperfection. In a crude attempt to simulate material degradation in the band, additional softening is assigned to the localized elements only *after* the shear band has formed. The effect of the additional softening is to sharpen the shear banding and enhance the localization pattern.

In contrast to the aforementioned results, in the paper by Belytschko et al. [8], the authors report that the initial bandwidth is set by the size of the imperfection, even in the dynamic case (in case of more than one band, in addition to the bandwidth, the shear band pattern varies with the size of the imperfection, i.e. the number of bands and their orientation change with the size of the imperfection). They also find that the shear band narrows with time. The continuing narrowing of the shear band gives rise to mesh dependent solutions, since ultimately even the finest possible mesh fails to resolve the band. The difference between the results reported in this paper and those due to Belytschko et al. [8] can be attributed to the fact that the visco-plastic constitutive relations of the power law type used by the latter lead to explosion of imperfections. Comparison of the adaptive meshing approach used in this paper with the enriched displacement procedure of Loret et al. [1] leads to interesting conclusions. It is found that the adaptive meshing and enriched displacement procedures yield consistent solutions. The

enriched displacement procedure requires that the characteristic size of the element in which the patch solution is performed, be at least one order of magnitude larger than the size of the putative band, $h/10\,c\eta > 10$. For smaller values of $h/10\,c\eta$, the adaptive meshing procedure is preferable. For $10\,c\eta$ several orders of magnitude smaller than $h$, the computational cost of adaptive meshing and stable time integration would render this approach extremely expensive: in such cases the enriched displacement procedure should be used. More usually, to resolve the structure of actual shear bands, we would expect a combination of both approaches to be particularly effective: several levels of adaptive mesh refinement followed by use of the enriched displacement procedure in the localized elements comprise a plausible scenario for tackling real-world problems.

While the adaptive meshing procedure yields consistent results, its capacity to resolve the structure of the shear band, in particular to give the correct band width, is hampered by the limitations associated with the need to transfer the state variables between successive meshes in all calculations involving history-dependent constitutive relations. As discussed in the above examples, the adaptive meshing procedure tends to predict values of the bandwidth somewhat larger than the expected value of $10\,c\eta$. While the procedure for transferring the state variables suggested in Section 5.2 was found to be more efficient than many of the methods currently in practice, there are undoubtedly limitations associated with it. The 'smoothing' process inevitably involves loss of information and smearing, thereby limiting the finite element's capacity to resolve the shear band. However, 'smoothing' cannot be entirely avoided, as otherwise the discontinuity at element boundaries results in 'noise' and corrupts the solutions.

Improved and more accurate stress recovery procedures appear to be the need of the hour. The further success of adaptive meshing schemes for strain localization type problems hinges on developments in this area.

## Acknowledgments

A. Deb would like to acknowledge the financial support from Phillips Petroleum Co. in the form of a graduate fellowship which partially supported his graduate studies at Princeton University.

## References

[1] B. Loret, J.H. Prevost and A. Deb, Finite Element simulation of dynamic strain localization: a multi scale problem, Comput. Methods Appl. Mech. Engrg. 120 (1995) 315–338.
[2] Z.P. Bazant and F.B. Lin, Non-local yield limit degradation, Int. J. Numer. Methods Engrg. 26 (1988) 1805–1823.
[3] N. Triantafyllidis and E.C. Aifantis, A gradient approach to localization of deformation: I. Hyperelastic materials, J. Elasticity 16 (1986) 225–237.
[4] H.B. Mühlhaus and I. Vardoulakis, The thickness of shear bands in granular materials, Geotechnique 37 (1987) 271–283.
[5] A. Needleman, Material rate dependence and mesh sensitivity in localization problems, Comput. Methods Appl. Mech. Engrg. 67 (1988) 69–85.
[6] B. Loret and J.H. Prevost, Dynamic strain-localization in elasto-visco-plastic solids: Part 1—General formulation and one-dimensional examples, Comput. Methods Appl. Mech. Engrg. 83 (1990) 247–273.
[7] L.J. Sluys and R. de Borst, The use of higher-order continuum models for the computational modeling of shear-banding, Mech. Mater. 18 (1994) 131–149.
[8] T. Belytschko, H.Y. Chiang and E. Plaskacz, High resolution two-dimensional shear band computations: imperfections and mesh dependence, Comput. Methods Appl. Mech. Engrg. 119 (1994) 1–15.
[9] T. Belytschko, J. Fish and B. Engelmann, A finite element with embedded localization zones, Comput. Methods Appl. Mech. Engrg. 70 (1988) 59–89.
[10] J. Fish and T. Belytschko, A finite element with a unidirectionally enriched strain field for localization analysis, Comput. Methods Appl. Mech. Engrg. 78 (1990) 181–200.
[11] T. Belytschko, J. Fish and A. Bayliss, The spectral overlay on finite elements for problems with high strain-gradients, Comput. Methods Appl. Mech. Engrg. 81 (1990) 71–89.
[12] M. Ortiz and J.J. Quigley IV, Adaptive mesh refinement in strain-localization problems, Comput. Methods Appl. Mech. Engrg. 90 (1991) 781–809.

[13] T. Belytschko and M. Tabbara, H-adaptive finite element methods for dynamic problems with emphasis on localization, Int. J. Numer. Methods Engrg. 36 (1993) 4245–4265.
[14] D. Peric, J. Yu and D.R.J. Owen, On error estimates and adaptivity in elasto-plastic solids: Applications to the numerical simulation of strain localization in classical and Cosserat continua, Int. J. Numer. Methods Engrg. 37 (1994) 1351–1379.
[15] O.C. Zienkiewicz, M. Huang and M. Pastor, Localization problems in plasticity using finite elements with adaptive remeshing, Int. J. Numer. Methods Engrg. 19 (1995) 127–148.
[16] T.J.R. Hughes, The Finite Element Method (Prentice-Hall, Englewood Cliffs, NJ, 1987).
[17] O.C. Zienkiewicz and J.Z. Zhu, The super-convergent patch recovery and a posteriori error estimates, Part 1: The recovery technique, Int. J. Numer. Methods Engrg. 33 (1992) 1331–1364.
[18] A.R. Diaz, N. Kikuchi, P. Palambros and J.E. Taylor, Design of an optimal grid for finite element methods, J. Struct. Mech. 11(2) (1983) 215–230.
[19] A. Deb, B. Loret and J.H. Prevost, An automated band identification procedure for dynamic strain localization, Comput. Methods Appl. Mech. Engrg. 137 (1996) 307–330.
[20] C. Lamouroux, P. Debat, N. Guerrero, J. Ingles, P. Sirieys and J.C. Soula, Analysis of natural ductile shear zones, Mech. Mater. 18 (1994) 79–87.
[21] S.H. Lo, Generating quadrilateral elements over plane and curved surfaces, Comput. Struct. 31 (1989) 421–426.
[22] L.R. Herrmann, Laplacian-Isoparametric grid generation scheme, ASCE J. Struct. Engrg. 51 (1976) 35–40.
[23] P. Devloo, J.T. Oden and T. Strouboulis, Implementation of an adaptive refinement scheme for the SUPG algorithm, Comput. Methods Appl. Mech. Engrg. 61 (1987) 339–358.
[24] N.E. Wiberg, F. Abdulwahab and S. Zuikas, Enhanced superconvergent patch recovery incorporating equilibrium and boundary conditions, Int. J. Numer. Methods Engrg. 37 (1994) 3417–3440.
[25] T. Blacker and T. Belytschko, Super-convergent patch recovery with equilibrium and conjoint interpolant enhancements, Int. J. Numer. Methods Engrg. 37 (1994) 517–536.
[26] D.P. Flanagan and T. Belytschko, Eigenvalues and stable time steps for the uniform strain hexahedron and quadrilateral, ASME J. Appl. Mech. 51 (1984) 35–40.
[27] J.H. Prevost and B. Loret, Dynamic strain-localization in elasto-(visco)-plastic solids: Part 2—Plane strain examples, Comput. Methods Appl. Mech. Engrg. 83 (1990) 275–294.
[28] T. Belytschko, B. Moran and M. Kulkarni, The crucial role of imperfections in quasi-static visco-plastic solutions, ASME J. Appl. Mech. 58 (1991) 658–665.
[29] K. Jansen, F. Shakib and T.J.R. Hughes, Fast projection for unstructured meshes, in: S.N. Atewi, ed., Computational Nonlinear Mechanics in Aerospace Engineering, Vol. 146 (American Institute of Aeronautics and Astronautics, 1992) Chap. 5.